

Article

# Co-Aromatization of n-Butane and Methanol over PtSnK-Mo/ZSM-5 Zeolite Catalysts: The Promotion Effect of Ball-Milling

Kang Yang , Lingting Zhu, Jie Zhang, Xiuchun Huo, Weikun Lai, Yixin Lian \* and Weiping Fang

National Engineering Laboratory for Green Chemical Productions of Alcohols-Ethers-Esters, College of Chemistry and Chemical Engineering, Xiamen University, Xiamen 361005, Fujian, China; yang\_kang\_1987@126.com (K.Y.); zhulingting1125@126.com (L.Z.); zhangjie0315666@126.com (J.Z.); chunxiu0212@163.com (X.H.); laiweikun@xmu.edu.cn (W.L.); wpfang@xmu.edu.cn (W.F.)

\* Correspondence: lianyx@xmu.edu.cn (Y.L.); Tel.: +86-592-2880786

Received: 3 July 2018; Accepted: 25 July 2018; Published: 28 July 2018



**Abstract:** The ball-milling (BM) method benefits the stabilization and dispersion of metallic particles for the preparation of the PtSnK–Mo/ZSM-5 catalyst. Based on the TPR, H<sub>2</sub>-TPD, XPS, and CO-FTIR results, the Pt–SnO<sub>x</sub> and MoO<sub>x</sub> species were formed separately on the BM sample. During the aromatization of cofeeding the n-butane with methanol, the yield of the aromatics is 59 wt.% at a n-butane conversion of 86% at 475 °C over the Pt Mo BM catalyst. The more weak acid sites also contribute to the aromatics formation with the less light alkanes formation. For the Pt Ga catalysts, the slow loss of activity suggests that the BM method can restrain the coke deposition on the Pt–SnO<sub>x</sub> species, because of a certain distance between the Pt–SnO<sub>x</sub> and GaO<sub>x</sub> species on the surface of ZSM-5.

**Keywords:** ball-milling; cofeeding; n-butane; methanol; aromatization

## 1. Introduction

According to a report from the Stanford Research Institute (SRI), both the capacity and consumption of benzene will increase to 66.59 million tons per year (TPY) and 50.99 million TPY, respectively, until 2019; the capacity of toluene will increase to 42.42 million TPY until 2018; and both the capacity and consumption of o-xylene will increase to 5.35 million TPY and 3.88 million TPY, respectively, until 2020 [1]. However, with the increasing demand for benzene, toluene, and xylenes (BTX), and the continuous petroleum consumption, the traditional petroleum refinery route is difficult to meet the demands of the BTX market. In this context, the methanol to aromatics (MTA) conversion, as a petroleum-free route, would be a highly attractive alternative [2]. The MTA conversion produced a variety of hydrocarbons via the dual cycles of the aromatics carbon pool and olefins carbon pool [3]. The loading of metal on ZSM-5 promoted the dehydrogenation processes to increase the yield of aromatics [4–6]. In this way, the weight ratio of the aromatics in the liquid organic product was around 90%, which is much higher than that in the methanol to gasoline (~35%) and that in the catalytic reforming of naphtha (50–65%) [7]. However, many problems still exist that control the exothermicity of this reaction and decrease the rapid deactivation [4,6]. Mier et al. [8] have combined the cracking of n-butane and methanol on a HZSM-5 zeolite catalyst to produce alkenes. It was proposed that the olefins from cracking played significant roles for both improving the methanol conversion and attenuating the coke formation. Recently, Song et al. [9] found that at a suitable n-butane/methanol ratio of 60/40, 480 °C, 0.4 MPa, WHSV (CH<sub>2</sub>) = 0.6 h<sup>-1</sup>, a high aromatics selectivity could be achieved. Increasing the methanol fraction in the feed, the coke content of the used catalyst increased and coke preferred to deposit in the micropore [10]. The introduction of the Mo species could increase the

reactive stability during many aromatization reactions [11–13]. Furthermore, the  $\text{Mo}_2\text{C}$  is also an effective promoter for the aromatization reactions over ZSM-5 [11,13,14]. Moreover, this catalyst can activate methane into benzene with an 80% selectivity at 10–15% conversion, while the Zn or Ga supported on ZSM-5 cannot do so [15].

In addition, the suitable preparation method is very important in order to take advantage of the active sites fully. ‘Mechanochemistry’, induced by the input of mechanical energy (grinding in ball mills), which is intensely studied because it can promote reactions between solids with either no added solvent or with only nominal amounts [16]. For example, Wang et al. [17] used ball-milling (BM) to combine a Zr–Zn binary oxide, which shows a higher selectivity to methanol and dimethyl ether at 400 °C, and SAPO-34 with a weaker acidity shows a ca. 70% selectivity to  $\text{C}_2$ – $\text{C}_4$  olefins at a ca. 10% CO conversion. Moreover, the Zn–Cr double metal cyanide complex (DMC) catalyst synthesized through the grinding method showed high catalytic activity during the alternating copolymerization of  $\text{CO}_2$  with propylene oxide [18], and it is interesting that ball-milled nanomaterials were so reactive that the conversion values are comparable with those of the microwave-prepared, supported iron oxide NPs, and impregnated materials for the oxidation of benzyl alcohol to benzaldehyde [19]. In this work, the proximity of the active components also plays a key role in this coupling reaction.

This paper describes a facile approach based on the ball-milling of typical Pt–Sn and Mo/Ga component supported on the ZSM-5 zeolite to produce ‘trifunctional catalysts’, because the intrinsic dehydrogenation property of Pt– $\text{SnO}_x$  is totally different from that of the  $\text{Ga}_2\text{O}_3$  and  $\text{MoO}_x$  active sites, where the successive dehydrogenation reaction of the cyclicalkenes is the main process to produce aromatics [4,20]; while Pt– $\text{SnO}_x$  is suitable for the dehydrogenation of n-butane [21]. The advantages of the potassium promoter have been reported in a butene oligomerization cracking mechanism by Zhu et al. [22] and Castaño et al. [23], indicating the lower deactivation by coke, as also proved with the olefin aromatization over the K modified ZSM-5 catalysts [24]. These prepared Pt Mo/Ga catalysts show better catalytical performance than those of the Pt Mo/Ga reference catalysts prepared by the impregnation method. The physical–chemical properties of the catalysts were studied by  $\text{N}_2$ -adsorption, X-ray fluorescence (XRF), X-ray diffraction (XRD), temperature programmed reduction (TPR), X-ray photoelectron spectrum (XPS),  $\text{NH}_3/\text{H}_2$ -temperature programmed desorption ( $\text{NH}_3/\text{H}_2$ -TPD), and in situ CO Fourier Transform infrared ray spectroscopy (CO-FTIR).

## 2. Results and Discussion

### 2.1. Catalyst Characterization

The adsorption properties are summarized in Table 1. At first, the introduction of promoters in a porous structure of zeolites did not lead to an insignificant decreasing of the surface area, pore volume, and pore diameter (Table S1). Secondly the BET surface areas, micropore areas, and volumes increased slightly (by ~5%) when the BM was used, consistent with the difference in the adsorption capacity (Figure S3A). It should be noted that the milling process can create more pores in the catalyst upon the BM process, according to previous mechanochemistry reports [19,25], which benefit the stabilization and dispersion of metallic particles, while all of the samples possessed similar mesopores (3–5 nm), in Figure S3B. The powder XRD patterns of the supported samples are shown in Figure 1 and Figure S2. Evidently, these diffraction patterns are almost identical to that of the typical ZSM-5 zeolite [26], confirming the retention of the highly crystalline of the ZSM-5, no matter what preparation method is used. After the Pt–Sn and Mo/Ga deposition, the reflection peaks of these metals or related compounds are not observed in the XRD patterns, probably due to the low loading and/or the high dispersion on the support.

**Table 1.** Textural properties and chemical composition of Pt Mo ball-milling (BM), Pt Mo impregnation (IMP), Pt Ga BM, and Pt Ga IMP samples.

Sample	XRF Analysis (wt.%)			$S_{BET}$ ( $m^2 \cdot g^{-1}$ )	t-Plot		
	Pt	Sn	Mo/Ga		$S_{micro}$ ( $m^2 \cdot g^{-1}$ )	$V_{micro}$ ( $cm^3 \cdot g^{-1}$ )	$D$ (nm)
Pt Mo IMP	0.45	0.93	1.44	333	246	0.093	2.7
Pt Ga IMP	0.46	0.92	1.46	324	242	0.092	2.8
Pt Mo BM	0.47	0.94	1.48	348	261	0.100	2.6
Pt Ga BM	0.46	0.93	1.45	341	252	0.095	2.7

$S_{BET}$ —surface area derived from the Brunauer–Emmett–Teller (BET)-method;  $S_{micro}$ —micropore surface area;  $V_{micro}$ —micropore volume;  $D$ —average pore diameter. XRF—X-ray fluorescence.

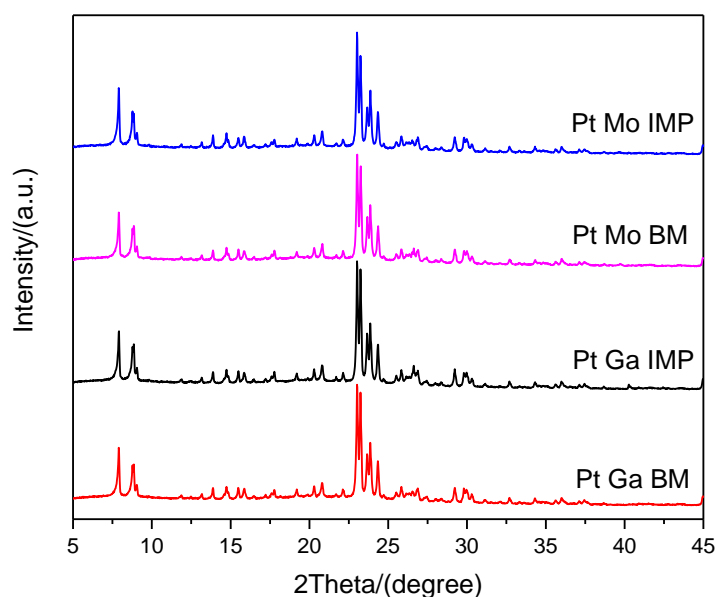
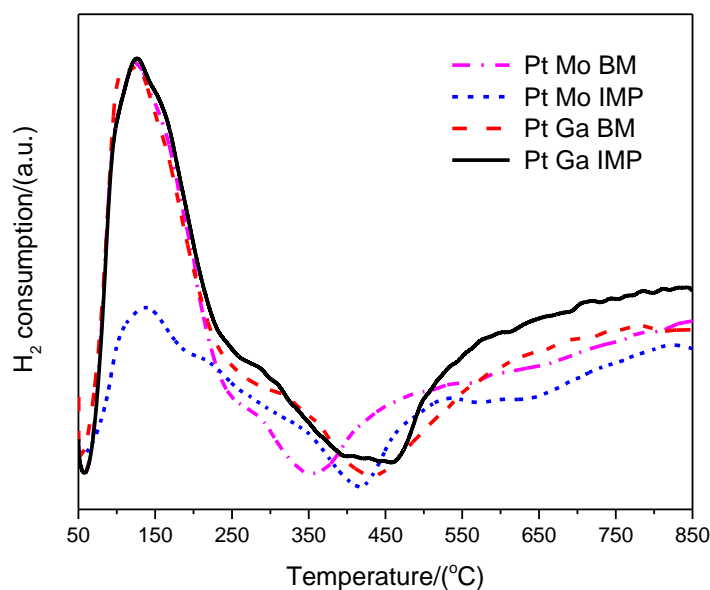
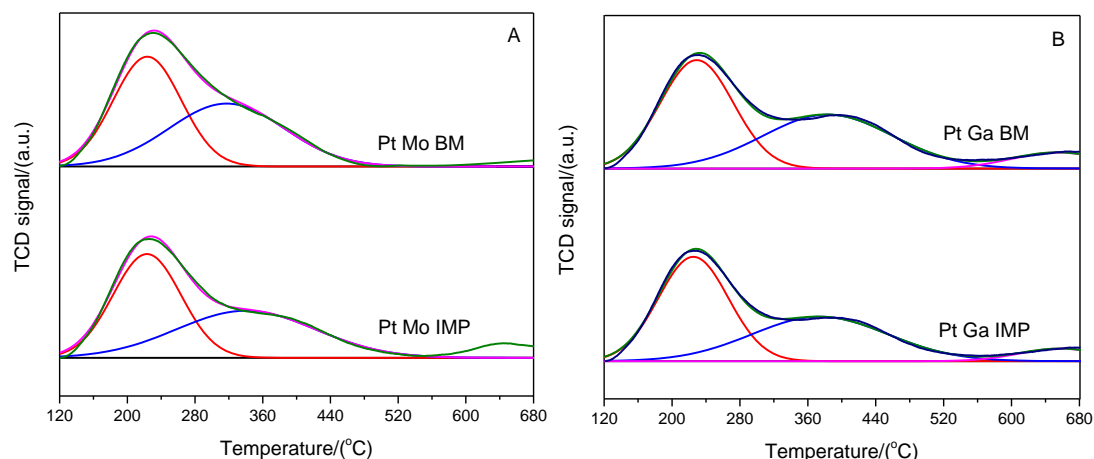
**Figure 1.** XRD patterns of Pt Mo and Pt Ga samples. All of the samples are reduced at 500 °C for 1 h. IMP—impregnation; BM—ball-milling.

Figure 2 shows the TPR profiles of the IMP and BM samples. The reduction profile for the Pt Mo BM sample (Dash dot) shows the following peaks: at ca. 150 °C, which corresponds to the Pt particles reduced to Pt<sup>0</sup> completely; at ca. 240 °C, attributed to the reduction of Pt interacting with the support [27,28]; and from 450 °C, attributed to reduction of MoO<sub>3</sub> and the complete reduction, as well as the metal-support interactions [28,29]. However, the intensity of the first reduction peak decreased significantly when the IMP was used. This behavior could be as a because the Pt surface was modified by the Mo species, because the latter is as three-fold as the former [28]. This modification will be discussed later using the CO-FTIR and XPS measurements. This contention was also proposed by Mériaudeau et al. [30], who showed that, at least for a small addition of the molybdenum precursor (molybdate), it is preferentially adsorbed on the platinum surface rather than the support. The effect of the migration MoO<sub>x</sub> phase onto the Pt species in the PtMo/Al<sub>2</sub>O<sub>3</sub> catalysts after reduction followed by passivation, has been reported by Pereira da Silva et al. [31]. Accordingly, the reduction of Pt is not complete on the Pt Mo IMP sample. On the contrary, the addition of Ga did not lower the reducibility of Pt oxide on the Pt Ga IMP sample. This might be attributed to the ligand, and the ensemble effects triggered by GaO<sub>x</sub> can be ignored. While the presence of platinum enhanced the reducibility of the Ga oxides, because the intensity above 550 °C increased obviously on the Pt Ga IMP sample.



**Figure 2.** H<sub>2</sub>-temperature programmed reduction (TPR) profiles of Pt Mo BM, Pt Mo IMP, Pt Ga BM, and Pt Ga IMP samples.

The acidity of the supported samples was tested by the NH<sub>3</sub>-TPD measurement. A typical NH<sub>3</sub>-TPD profile of ZSM-5 shows two peaks centered at a low temperature (ca. 250 °C) and at a high temperature (>360 °C). The former peak is assigned to the desorption of ammonia from weak acid sites and the latter peak is due to the desorption of ammonia from strong acid sites [7,26,27]. However, the introduction of promoters leads to an insignificant decrease of strong acid sites, suggesting that the addition of potassium can neutralize the strong acid sites preferentially and that the loading of promoters could consume strong acid sites by the dehydration process under the influence of calcination, as shown in Figure S4 [32,33]. As shown in Figure 3, the concentration of acid sites decreased when the IMP was used, consistent with the decrease in the N<sub>2</sub> adsorption capacity (Figure S3). One other explanation is that half of the ZSM-5 support was only impregnated by a Mo or Ga precursor solution for the BM samples, while the whole support of the IMP samples was first impregnated by a Mo or Ga precursor solution (KCl was also included) and then a Pt–Sn precursor solution. During impregnation, the zeolitic proton was exchanged by alkali metal (K) species [34]. Thus, a certain amount of acid sites can be survived on that half of the ZSM-5 support that was only impregnated once. In addition, the amount of weak acid is much more than that of the strong acid on all of the samples. After deconvoluting the peaks, the strong acid sites on the Pt Ga samples are more obvious than those on the Pt Mo samples. Additionally, the peak temperatures of the strong acid sites are higher than 360 °C on the Pt Ga samples; while these temperatures are almost lower than 360 °C on the Pt Mo samples. It is well known that the β-Ga<sub>2</sub>O<sub>3</sub> component also has large amounts of acidic sites, which are active for the propane dehydrogenation [20].



**Figure 3.**  $\text{NH}_3$ -TPD profiles of Pt Mo BM and Pt Mo IMP (A), and Pt Ga BM and Pt Ga IMP (B) samples.

The characteristics of chemisorbed hydrogen were studied by the temperature programmed desorption of hydrogen ( $\text{H}_2$ -TPD). The  $\text{H}_2$ -TPD profiles obtained after the  $\text{H}_2$  chemisorption at  $50^\circ\text{C}$  over the Pt Mo/Ga samples, are shown in Figure 4. All of the samples show a broad desorption peak below  $450^\circ\text{C}$ , and this peak is centered at ca.  $250^\circ\text{C}$  and  $350^\circ\text{C}$  for the Pt Mo and Pt Ga samples, respectively. Although the decrease in the reduction peak of Pt is obvious on the Pt Mo IMP (Figure 2), the decrease in the  $\text{H}_2$ -TPD peak is not significant. Ro et al. [35] found that the presence of the Pt– $\text{MoO}_x$  sites enhanced the catalytic activity over the PtMo/ $\text{SiO}_2$  catalysts, and Matsuda et al. [36] has shown that  $\text{H}_2$  reduction of Pt/ $\text{MoO}_3$ – $\text{SiO}_2$  converts the  $\text{MoO}_3$  into  $\text{MoO}_x\text{H}_y$  species, which are active for dehydrogenation. Besides the Pt– $\text{SnO}_x$  active species, the Pt–Mo interfacial sites were also produced over the Pt Mo IMP sample after a  $500^\circ\text{C}$  reduction. While on the Pt Mo BM, the main metal sites for dehydrogenation are Pt– $\text{SnO}_x$  (ca.  $250^\circ\text{C}$ ) and  $\text{MoO}_x$  (ca.  $650^\circ\text{C}$ ) species, which are located separately on half of ZSM-5 support. However, it is very interesting that the  $\text{H}_2$  desorption behaviors for Pt Ga samples are almost the same. The reduction of Pt on those samples are as complete as that on Pt Mo BM, while both desorption peaks become wider and shift to higher temperatures (ca.  $350^\circ\text{C}$ ). Pidko et al. [37] in their DFT study, showed that the regeneration of the active  $\text{GaO}^+$  by the  $\text{H}_2$  desorption from  $\text{H-Ga-OH}^+$  was not favorable. Other desorption profiles above  $450^\circ\text{C}$  can be related to the  $\text{H}_2$  chemisorption on the Mo and Ga oxides.

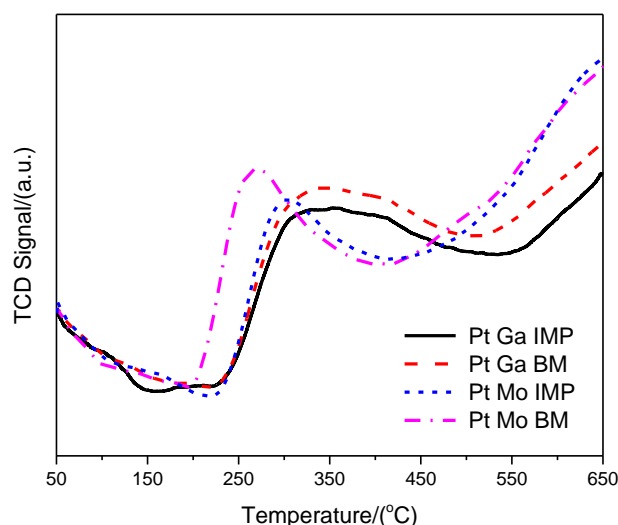


**Figure 4.**  $\text{H}_2$ -TPD profiles of Pt Mo BM, Pt Mo IMP, Pt Ga BM, and Pt Ga IMP samples.

Figure 5 shows the infrared spectra of the CO chemisorbed on the Pt Mo/Ga samples, collected at ca. 30 °C after in situ reduction. The total peak of the Pt Mo IMP almost disappeared, while the Pt Mo BM shows the strong CO adsorption (Figure 5a,b), consistent with the TPR result (Figure 2). This might be caused by some Mo species, which occupied the active sites of Pt–SnO<sub>x</sub> for the CO adsorption, and active Pt–Mo interfacial sites that were not sensitive in the flowing CO at room temperature. This difference further demonstrates that the active Pt–SnO<sub>x</sub> species on half of the ZSM-5, for either the H<sub>2</sub> or CO adsorption, were not influenced by MoO<sub>x</sub> over the Pt Mo BM sample. However, the total peak area of the Pt Ga IMP (Figure 5c) is much higher than the Pt Mo IMP. It should be noted that the dihydrogen molecules were demonstrated to be dissociated over Ga<sub>2</sub>O<sub>3</sub> into the H<sup>+</sup> and H<sup>−</sup> species after the H<sub>2</sub> reduction [20]. Similarly, the active Pt–SnO<sub>x</sub> species on half of the ZSM-5 for the CO adsorption were not influenced by GaO<sub>x</sub> over the Pt Ga BM sample, as shown in Figure 5d,e.

The spectra of the Pt Mo/Ga BM samples are asymmetrical and can be deconvoluted into three peaks. They are near 2173 cm<sup>−1</sup>, 2082 cm<sup>−1</sup>, and a shoulder peak near 2110 cm<sup>−1</sup>. Arai et al. attributed a band at 2080 cm<sup>−1</sup> and a shoulder band at 2040 cm<sup>−1</sup> to the CO adsorbed on the Pt terrace sites and on the Pt edge, corner, and/or kink sites, respectively [38]. The lower frequency band can be related to the CO adsorbed on the under-coordinated sites and the high frequency band to terrace sites [39]; while the band at 2070–2090 cm<sup>−1</sup> was also assigned to the CO linearly adsorbed on the surface of the Pt crystal in other studies [40]. Because the binding energy of Pd 3d<sub>5/2</sub> for the Pd–Sn bimetallic is shifted towards a higher binding energy with a maximum at 335.3 eV [41], the inadequate electrons backdonation from the metal to the empty π\*-type orbitals of the CO can be accepted. The IR band at ca. 2173 cm<sup>−1</sup> should be ascribed to the linear CO species on the Pt–SnO<sub>x</sub> species without a d-π\* backdonation, because of the stretching frequency measured at 2143 cm<sup>−1</sup> for the free CO molecule in the gas [42]. This kind of adsorption was also observed on the Mo/SnO<sub>2</sub> sample [43]. After comparison, the Pt Mo BM showed a similar CO-FTIR band to that of the Pt Ga BM sample. Therefore, the difference in the catalytical performance of these samples should be mainly originated from the intrinsic difference in the activities of the MoO<sub>x</sub> and GaO<sub>x</sub> species.

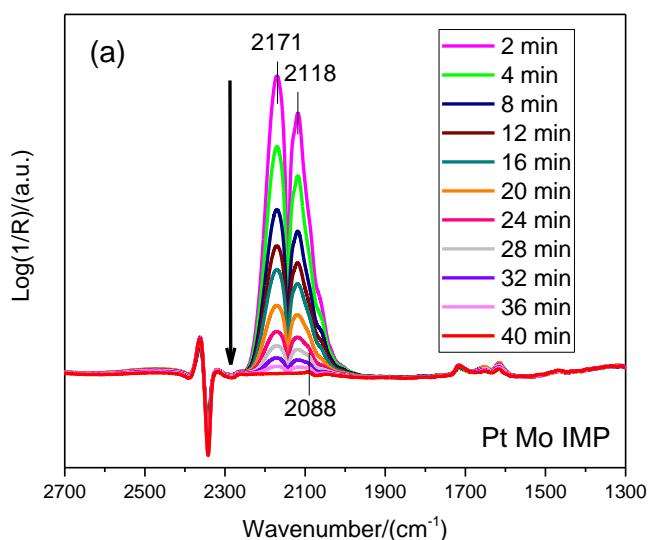


Figure 5. Cont.

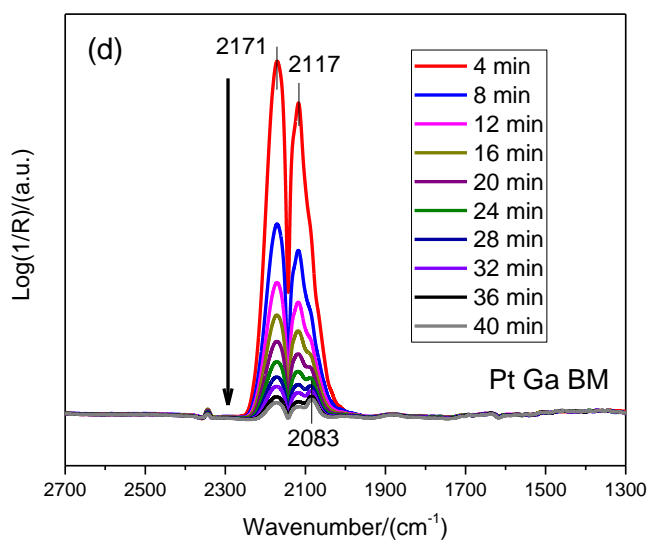
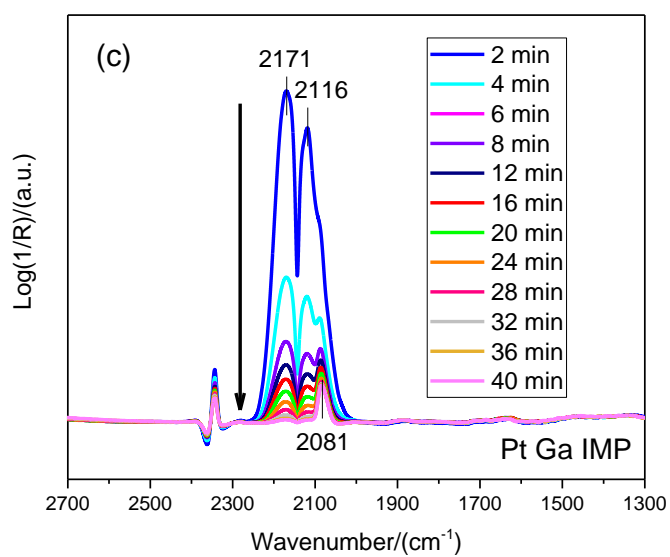
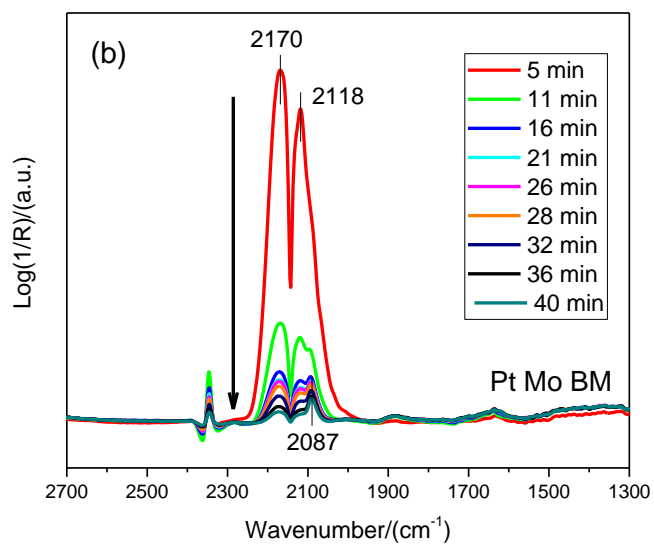
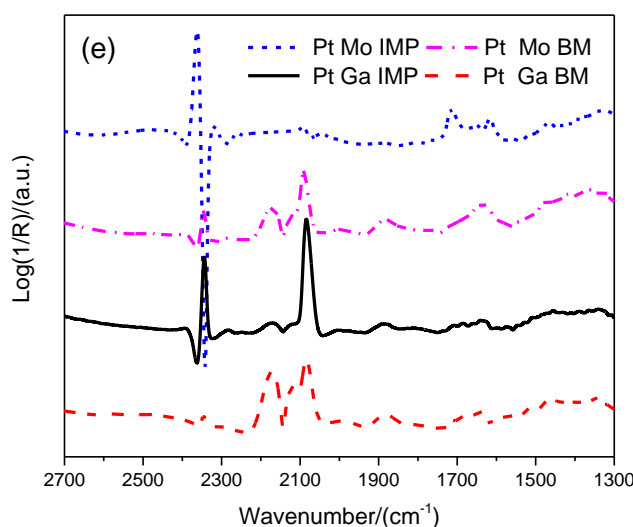


Figure 5. Cont.



**Figure 5.** Evolution of the in situ CO-FTIR spectra of the Pt Mo IMP (a), Pt Mo BM (b), Pt Ga IMP (c), and Pt Ga BM (d) under  $N_2$  during 40 min, and the stable spectra of these samples (e). All of the samples are in situ reduced at  $500\text{ }^\circ\text{C}$ .

To investigate the chemical state of the metal components, XPS analyses were carried out. The energy regions of the Pt (4d), Sn (3d), Mo (3d), and Ga (2p) core levels in the reduced (at  $500\text{ }^\circ\text{C}$ ) samples were recorded. Figure 6A shows the Pt  $4d_{5/2}$  spectra after deconvolution. Although the most intense photoemission lines of platinum were those arising from the Pt 4f levels [44], this energy region was overshadowed by the presence of a very strong Al 2p peak, and thus the Pt 4d lines were analyzed instead [45]. In general, the signal at the higher binding energy (316.0–317.1 eV) can be ascribed to the  $PtO_2$  species [46], whereas the second band at the lower binding energy (314.3–315.5 eV) can be assigned to the presence of the  $Pt^0$  species [45]. All of the samples show only the BE values of the metallic Pt particles. Furthermore, the binding energy of the Pt  $4d_{5/2}$  for the BM samples is shifted towards a higher binding energy (ca. 314.5  $\rightarrow$  315.3 eV), which can explain their CO-FTIR spectrum with almost no  $d-\pi^*$  backdonation.

When two Mo  $3d_{5/2}$ –Mo  $3d_{3/2}$  doublets were considered, the spectra for the Pt Mo samples (Figure 6B) show two well resolved spectral lines at 232.5 and 235.6 eV, which correspond to the Mo  $3d_{5/2}$  and Mo  $3d_{3/2}$  orbitals of the  $Mo^{6+}$  species, respectively [47,48]. The less intense peaks, with binding energy at 230.3 and 233.5 eV for the Mo  $3d_{5/2}$ –Mo  $3d_{3/2}$  doublet, are linked with the presence of  $Mo^{4+}$  [48]. The reduction of  $Mo^{6+}$  to  $Mo^{4+}$  is not efficient on both of the Pt Mo samples, while the fraction of  $MoO_2$  on Pt Mo BM is more than that on the Pt Mo IMP sample. The complete reduction of Pt on the Pt Mo BM may promote the reduction of  $MoO_3$ . Moreover, two Ga  $2p_{3/2}$ –Ga  $2p_{1/2}$  doublets were also considered, as shown in Figure 6C. The spectra for the Pt Ga samples show two well resolved spectral lines at 1118.2 and 1145.0 eV, which correspond to the Ga  $2p_{3/2}$  and Ga  $2p_{1/2}$  orbitals, respectively [49]. These peaks indicate the presence of  $Ga_2O_3$ . In addition, the higher BE values than the characteristic of the pure  $Ga_2O_3$  (1117.8 eV) indicated a more ionic character of the Ga–O bond [50]. Furthermore, only a very small amount of metallic Ga was observed on both of the Pt Ga samples. Because there is no obvious difference in the Sn  $3d_{5/2}$  spectra and only one Sn  $3d_{5/2}$  component was observed in our catalyst system, that is the component at the binding energy of 487.1–487.6 eV, which was attributed to oxidized tin (II, IV) [44]. Any peaks related to zerovalent tin, Sn in the Pt–Sn alloy, and chlorinated tin were not detected, as shown in Figure S5. Therefore, the Pt– $SnO_x$  species were proved on the BM catalysts and are the main active sites for n-butane dehydrogenation. Some parts of them were influenced by  $MoO_x$  or  $GaO_x$  on the IMP samples.

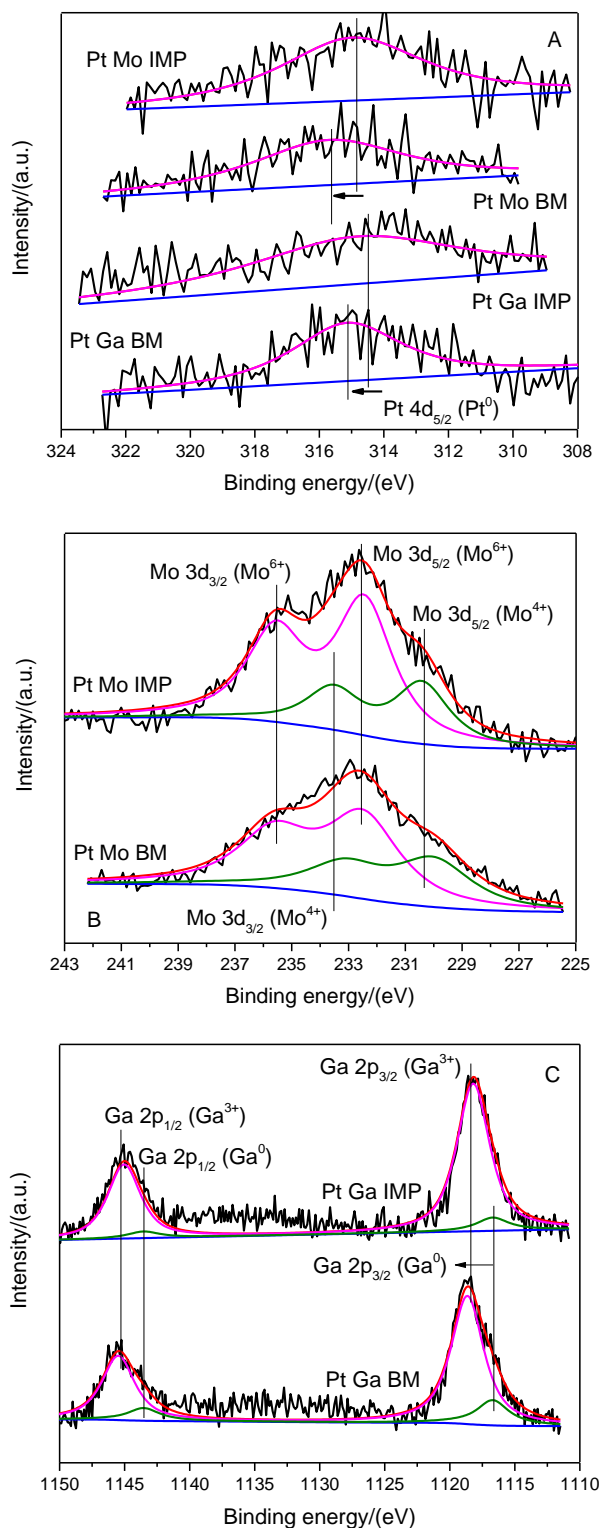


**Figure 6.** X-ray photoelectron spectrum (XPS) spectra of the Pt 4d (A), Mo 3d (B), and Ga 2p (C) regions for the Pt Mo/Ga samples. All of the samples are reduced at 500 °C.

## 2.2. Influence of Preparation Method on the Aromatization of Cofeeding *n*-Butane with Methanol

Table 2 lists the influence of the preparation method on the catalytical performance of co-aromatization with methanol at *n*-butane/methanol of 60/40, which has been proved as the best ratio for this cofeeding reaction [9,10]. During the aromatization of cofeeding methanol with

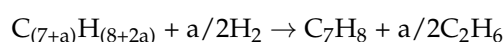
n-butane, methanol is fully converted. The Pt Mo BM shows the highest aromatics yield (45 wt.%), followed by the Pt Mo IMP (41 wt.%). Both of their values are higher than those of the Pt Ga catalysts. Hutchings et al. [4] attributed the advance in the MTA performance over the metal oxide-doped ZSM-5 to their higher activity in the propylene aromatization. However, Scurrall et al. [12] found that the Mo/ZSM-5 showed a higher cracking activity during the aromatization of n-hexane. As shown in Table 2, the total yield (17.2 wt.%) to the C<sub>2</sub>–C<sub>4</sub> alkanes of the Pt Mo BM is almost twice that (8.8 wt.%) of the Pt Mo IMP. It could be inferred that the MoO<sub>x</sub> species were modified by Pt–SnO<sub>x</sub> over the Pt Mo IMP so that the dehydrocyclization process was enhanced, leading to its promoting effect on aromatics formation. After comparison, the BM method seems to contribute little to the aromatization of light alkanes. While the dehydrogenation of the n-butane over the Pt Mo BM was favored because the reduction of Pt was complete (Figure 2), and the active Pt–SnO<sub>x</sub> species on half of the ZSM-5 were not influenced by MoO<sub>x</sub>, as shown in Figures 4 and 5. For the Pt Ga samples, both of the conversions of n-butane are lower.

**Table 2.** Pt Mo/Ga catalysts performance in the aromatization of cofeeding n-butane with methanol.

Catalyst	Pt Mo IMP	Pt Mo BM	Pt Ga IMP	Pt Ga BM
n-Butane conversion (%)	62	69	58	51
<i>Hydrocarbons distribution of reactor effluent (wt.%)</i>				
CH <sub>4</sub>	3.3	1.5	4	1.5
C <sub>2</sub> H <sub>6</sub> + C <sub>3</sub> H <sub>8</sub> + i-C <sub>4</sub> H <sub>10</sub>	8.8	17.2	17	15
C <sub>2</sub> H <sub>4</sub> + C <sub>3</sub> H <sub>6</sub> + C <sub>4</sub> H <sub>8</sub>	3.1	2.4	3	5.5
n-C <sub>4</sub> H <sub>10</sub>	38	31	42	49
CO + CO <sub>2</sub> + H <sub>2</sub> + C <sub>2</sub> H <sub>6</sub> O	2.3	1.4	2	2.4
C <sub>5</sub> + aliphatics	3.5	1.5	3	1.9
Aromatics	41	45	29	24.7
<i>Aromatics selectivity (wt.%)</i>				
Benzene	2.5	2	5.3	3.5
Toluene	12.3	17.9	21.5	18.7
Xylenes + ethylbenzene	50.8	52.8	50.2	54.2
C <sub>n≥9</sub> aromatics	34.4	27.3	23	23.6

Reaction conditions: 425 °C, 0.6 h<sup>-1</sup>, 0.2 MPa, time-on-stream (TOS) = 4 h, and n-butane/methanol = 60/40.

In order to increase the conversion of the n-butane and aromatics yield, this coupling reaction should be performed at a higher temperature; it is well known that the reaction temperature has a significant effect on controlling the product selectivity and aromatics distribution [9,15]. As shown in Figure 7, in the temperature range of 400–500 °C, the n-butane conversion increases with the temperature increasing, as all of the alkanes, except methane, can be activated more easily at a high temperature. Because propylene, ethylene, and butene appear only in traces (Table 2), only the selectivities to the alkanes were plotted in Figure 7A. The selectivity to ethane increases obviously and then decreases dramatically. Simultaneously, the selectivities to the C<sub>8</sub>–C<sub>9</sub> aromatics decrease and then increase (Figure 7B). Besides the cracking and hydrogen transfer, the side-chain hydrogenolysis of bulky aromatics molecules can also produce small alkanes with aid of H<sub>2</sub> [51,52]. For example,



Therefore, besides propylene aromatization [4], the dehydrogenation of ethane can also contribute to the aromatics production. After that, all of the alkanes participated in the aromatization, except for methane. The obvious increase in the methane production with the reaction temperature indicates that cracking is also favored, as the cracking of alkanes is endothermic. Besides the hydrogenolysis of bulky aromatics molecules, dealkylation can also occur because of an obvious decrease in the C<sub>8</sub>–C<sub>9</sub> aromatics formation between 425–475 °C. For instance, the C<sub>6</sub>H<sub>5</sub><sup>+</sup> species, which is formed via the demethylation

of polymethyl aromatics, could connect with the zeolite framework to compensate for the negative charge in the acid sites, hindering the passage of the reactants and products, and decreasing the reactivity of the catalyst [51]. Therefore, the conversion (ca. 60%) increases very slowly and almost remains constant in this temperature range.

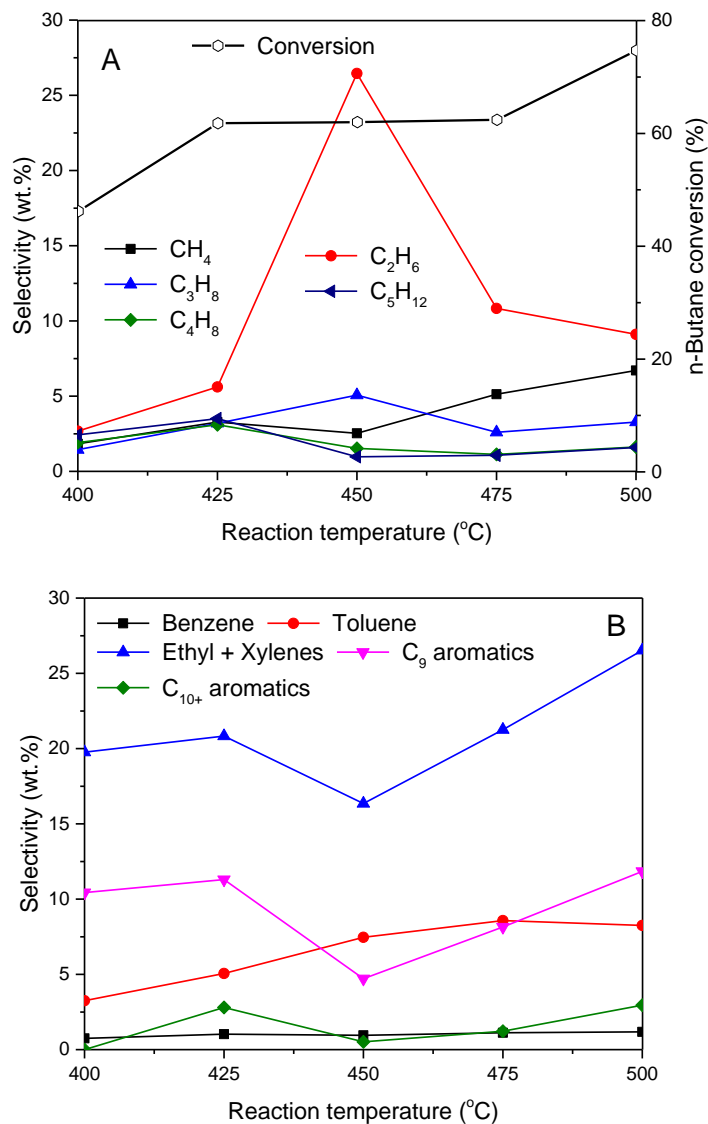


**Figure 7.** Effect of reaction temperature on n-butane conversion, selectivity to aliphatics (A), and selectivity to aromatics (B) over Pt Mo IMP. The C<sub>5</sub>H<sub>10</sub> in the aliphatics and C<sub>10</sub>H<sub>14</sub> in the aromatics were used to simplify the molar calculations for the C<sub>5</sub> aliphatics and C<sub>10+</sub> aromatics.

The aromatization of methanol is an exothermic reaction, while that of n-butane is an endothermic one. When the endothermic aromatization dominates, for example, on the Pt Mo BM catalyst, raising the temperature benefits the aromatization process, leading to a decrease in the alkanes selectivity (Figure 8A), as well as an increase in the aromatics selectivity (Figure 8B), and vice versa. For one thing, the active Pt–SnO<sub>x</sub> species for the n-butane dehydrogenation on half of the ZSM-5 were not influenced by MoO<sub>x</sub>, as shown in Table 2. For another thing, raising the temperature also benefits the diffusion of the light alkanes and small olefins from the Pt–SnO<sub>x</sub> species to the MoO<sub>x</sub> active sites for the following dehydrocyclization process. It is easy to understand that as these olefins were consumed by the aromatization steps, the dehydrogenation reaction was driven, so that the n-butane conversion increased evidently. This push is an example of Le Chatelier's principle [53]. Moreover, the presence

of a hysteresis loop in the isotherms, in Figure S3A, indicates the presence of mesopores in zeolite, and thus enhances the transport of the molecules at higher conversions [54]. After a comparison, the conversions of n-butane are apparently higher than those of Pt Mo IMP when the reaction temperature is above 450 °C. Thus, the advantage of the BM method is significant when the reaction temperature is high. In this case, a high reaction temperature also improves the production of the  $C_{n \geq 8}$  aromatics. Although the demand of benzene, toluene, and xylenes (BTX) is gaining importance because of fossil fuel depletion [6], the demand of para-xylene (PX) and 2,6-dimethylnaphthalene (2,6-DMN) among heavy aromatics is also important and is growing [7,55]. Taking a suitable selectivity to methane and a higher selectivity to the  $C_8$  aromatics into consideration, the suitable reaction temperature for Pt Mo BM catalyst is 475 °C.

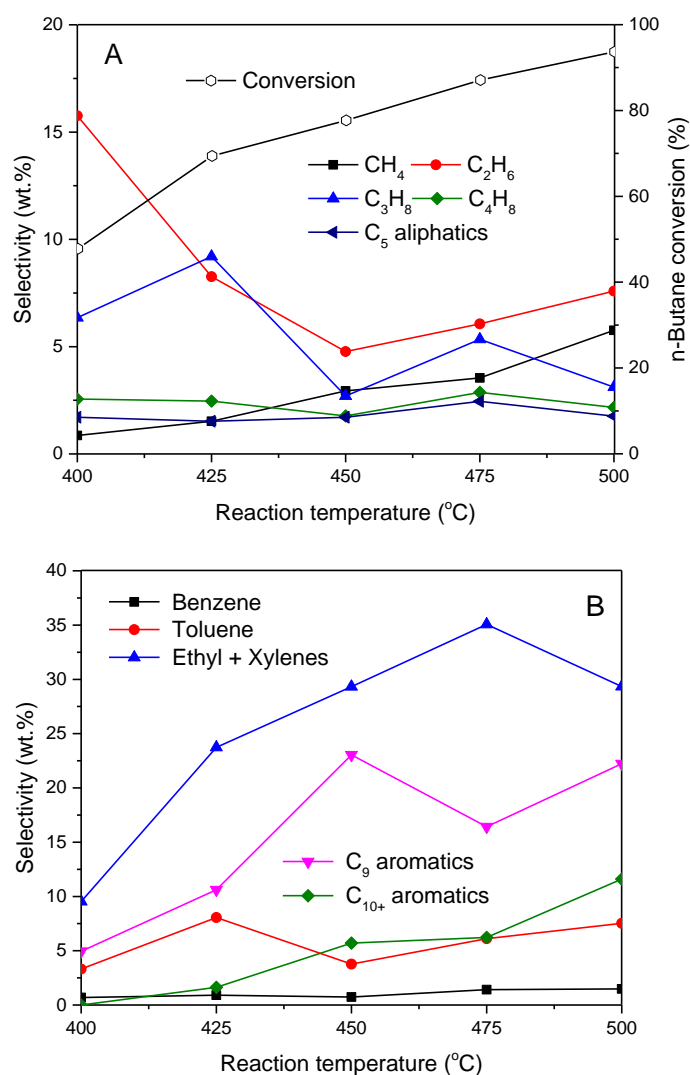


**Figure 8.** Effect of reaction temperature on n-butane conversion, selectivity to aliphatics (A), and selectivity to aromatics (B) over Pt Mo BM. The  $C_5H_{10}$  in aliphatics and  $C_{10}H_{14}$  in aromatics were used to simplify the molar calculations for the  $C_5$  aliphatics and  $C_{10+}$  aromatics.

The effects of the reaction temperature on the Pt Ga catalysts were also investigated and are shown in Figures S6 and S7 in the supporting information. It is obvious that the cracking to methane and ethane is enhanced when the reaction temperature is above 450 °C over the Pt Ga BM catalyst (Figure S7), due to more strong acid sites than that of the Pt Ga IMP catalyst, as shown in Figure 4. It proves that the consumption of small alkanes and olefins were not preferentially over the  $GaO_x$

species. Although most of the light alkanes participate in aromatization over the Pt Ga IMP catalyst, the reactive stability decreases dramatically at a higher temperature (Figure S6). It has been proven that the prolonged lifetime of Ga/ZSM-5 in the MTA is demanding, because of more severe and harder coke deposition, making the catalyst regeneration challenging [5]. Therefore, the Pt–Mo interfacial sites are more active and stable than the Pt–Ga interfacial sites in the n-butane conversion over the IMP catalysts. However, the activity of the Pt Ga BM decreases slowly and is higher than that of the Pt Ga IMP catalyst above 450 °C. This might be attributed to the active Pt–SnO<sub>x</sub> species on half of the ZSM-5, which were not influenced by the polyalkyl monoaromatics or/and polyaromatics formed on GaO<sub>x</sub> simultaneously. In this case, the aromatization reactions can still occur over the Brønsted acid sites [20,56]. Thus, the difference in the loss of activity suggests that the BM method can restrain the coke deposition on the Pt–SnO<sub>x</sub> species, because there is a certain distance between the two active sites. Taking the higher conversion of n-butane and the selectivity to the C<sub>8</sub> aromatics, the suitable reaction temperature for the Pt Ga BM catalyst is 450 °C. Thus, the optimized evaluation results of the Pt Mo/Ga catalysts and one catalyst from another work are shown in Table 3.

**Table 3.** The Pt Mo/Ga and Zn/CDM5 catalysts performance in the aromatization of cofeeding n-butane with methanol at the optimized reaction temperature.

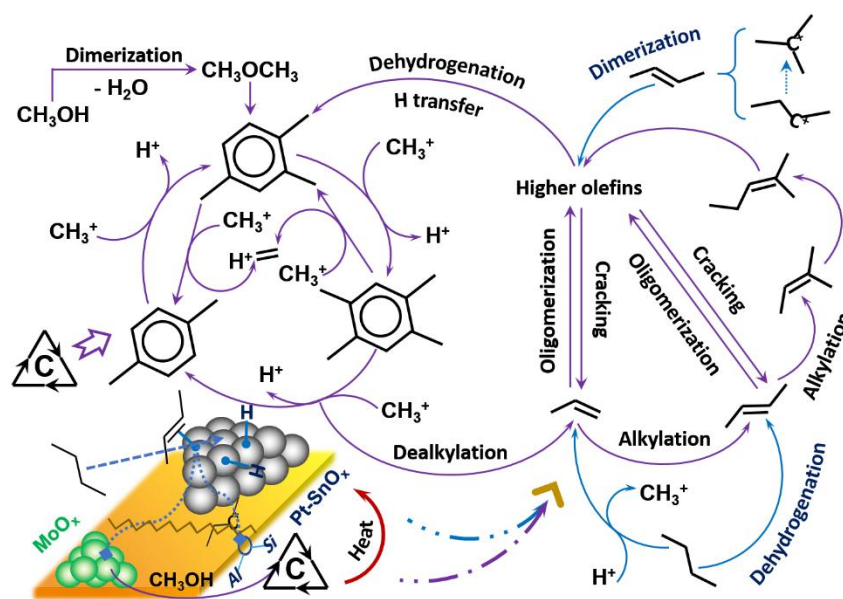
Catalyst	Pt Mo IMP	Pt Mo BM	Pt Ga IMP	Pt Ga BM	Zn/CDM5 *
Reaction temperature (°C)	475	475	450	450	480
n-Butane conversion (%)	65	86	74.7	76	62.7
<i>Hydrocarbons distribution of reactor effluent (wt.%)</i>					
CH <sub>4</sub>	4.8	1.3	4.1	4.2	2.89
C <sub>2</sub> H <sub>6</sub> + C <sub>3</sub> H <sub>8</sub> + i-C <sub>4</sub> H <sub>10</sub>	12.6	16.5	26.3	12.2	23.3
C <sub>2</sub> H <sub>4</sub> + C <sub>3</sub> H <sub>6</sub> + C <sub>4</sub> H <sub>8</sub>	1.1	3.5	5	2	7.33
n-C <sub>4</sub> H <sub>10</sub>	35	14	25.3	24	37.3
CO + CO <sub>2</sub> + H <sub>2</sub> + C <sub>2</sub> H <sub>6</sub> O	1.2	1.0	2	1.6	1.94
C <sub>5</sub> + aliphatics	1.3	0.7	3.3	2	1.57
Aromatics	38	59	26	48	25.67
<i>Aromatics selectivity in the liquid product (wt.%)</i>					
Benzene	2.8	5.3	6.6	2.0	7.7
Toluene	21.2	15.7	26.4	14.0	37.6
Xylenes + ethylbenzene	52.7	60.0	49.0	47.0	38.0
C <sub>n≥9</sub> aromatics	23.3	19	18	37.0	16.7
Coke (mg/g.cat.)	101	80	120	100	160

Reaction conditions: 0.6 h<sup>-1</sup>, 0.2 MPa, TOS = 4 h, and n-butane/methanol = 60/40. \* The reaction performance of Zn/CDM5 was adapted from Song et al. [9].

The Zn loading of Zn/CDM5 is ca. 2 wt.% and the support is the ZSM-5/ZSM-11 zeolite with a SiO<sub>2</sub>/Al<sub>2</sub>O<sub>3</sub> molar ratio of 50, which has a higher BET specific area than those of the catalysts in this work [9,57]. However, both the n-butane conversion (62.7%) and aromatics yield (25.7 wt.%) are lower than those of the Pt Mo/Ga catalysts. It is reasonable that the noble metal-platinum has a very high dehydrogenation/hydrogenation activity. An addition of platinum accelerates the dehydrogenation reactions and leads to a higher activity and a higher aromatic yield. It has been proven that the Pt–Sn/Mo/HZSM-5 catalysts enhance the formation of aromatic compounds and decreased the amount of coke during the aromatization of methane [29]. As shown in Table 3, both the n-butane conversion (86%) and aromatics yield (59 wt.%) of the Pt Mo BM catalyst are higher than those of the other catalysts, while the n-butane conversion (65%) of the Pt Mo IMP is much lower. After the thermogravimetric analysis (TG) measurement (Figure S8), the content of coke was calculated. It is obvious that the amounts of coke of the BM samples are lower than those of the IMP samples and the reference Zn/CDM5 catalyst. Therefore, a suitable preparation method is very important in order to take advantage of the active sites fully. For example, two active sites (Pt–SnO<sub>x</sub> and MoO<sub>x</sub>) should be

deposited on ZSM-5 independently, and an intimate contact between them has detrimental effects on each other. The co-aromatization performance of ZSM-5 at 450 °C and 475 °C for 4 h was also investigated, and is shown in Table S2. Both of the n-butane conversions are much lower (<40%) as well as the yields of the aromatics (<15 wt.%) without promoters. The main product is the C<sub>2</sub>–C<sub>3</sub> alkanes from the cracking and hydrogen transfer.

The effect of the Mo content on the aromatization of cofeeding the n-butane with methanol was further investigated, as shown in Table S3. It is obvious that the suitable Mo content is in the range of 0.5–1.5 wt.%, because of both the high n-butane conversion (ca. 85%) and high aromatics yield (ca. 50–60 wt.%). A higher Mo content (≥2.0 wt.%) might affect the activity of Pt–SnO<sub>x</sub>, so that the dehydrogenation of the n-butane was not favored. This proposal was proven by the CO-FTIR measurement, as shown in Figure S9. The stable CO adsorption behavior over the Pt Mo (3.0 wt.%) BM is very close to that of the Pt Mo IMP sample. In the suitable Mo content range, an increased Mo distribution makes a contribution to the aromatics production. Therefore, the optimized Mo content is 1.5 wt.%, due to the higher aromatics yield. Based on the Pt Mo (1.5 wt.%) BM catalyst, the surplus thermal energy released from the aromatization of methanol over the MoO<sub>x</sub> species could be available to the process of the dehydrogenation of alkane over Pt–SnO<sub>x</sub>. In turn, some small alkenes from the Pt–SnO<sub>x</sub> species can also participate in the reaction network of MTA, to promote the formation of higher olefins and propylene, as shown in Scheme 1. Therefore, the formation of the aromatics was also accelerated.



**Scheme 1.** Expected reaction paths over Pt Mo ball-milling (BM) catalyst during the aromatization of cofeeding n-butane with methanol.

The influence of the cofeeding composition on the reaction performance was investigated to prove this assumption. The detailed product distribution is presented in Table S4. With the increase of the methanol fraction, both the n-butane conversion and aromatics yield increased obviously with the gradual decrease in the yield to the light alkanes, while the aromatics yield is only 50 wt.% when pure methanol was fed. It has been suggested that noble metals like Pd, Ir, and Ru did not display any enhanced selectivity to aromatics during MTA [4]. On the contrary, the olefins formed from the n-butane transformation over Pt–SnO<sub>x</sub> can promote the process of MTA and vice versa, because the cracking of n-butane is the main process in the aromatization of the pure n-butane. In fact, the MTA is a very complicated process that includes the dehydration of methanol, formation of a hydrocarbon pool, and the production of aromatics and byproducts (light olefins and paraffins) through

a ‘dual-cycle’ mechanism [3,7,56]. During co-aromatization, the propene from the butane cracking and the butenes form butane dehydrogenation, and can also promote this ‘dual-cycle’ mechanism. Moreover, some methanol and n-butane could be adsorbed and consumed on Pt–SnO<sub>x</sub> and MoO<sub>x</sub>, respectively. Thus, the methanol dehydration over the Pt–SnO<sub>x</sub> and the protolysis-dehydrogenation of the n-butane nearby MoO<sub>x</sub> were also involved over the Pt Mo BM catalyst.

### 2.3. PtSnK–Mo/ZSM-5 Catalyst Stability for Co-Aromatization

To investigate the thermal stability, only the Pt Mo BM and Pt Mo IMP catalysts were subjected to long period tests under the best operating conditions of 475 °C, 0.2 MPa, and 0.6 h<sup>−1</sup>, because of the lower coke content on the Pt Mo catalysts. As shown in Figure 9A, the conversion of n-butane over the Pt Mo IMP increases from 60% to 85% and keeps the content for ca. 4 h and then decreases with the time-on-stream (TOS). Simultaneously, the total yield to the BTX products shows a similar change with TOS. Instead, the yield to gas products (C<sub>1</sub>–C<sub>4</sub> olefins and paraffins, the non-reacted n-butane was not included) decreases when the conversion is higher, and increases at the beginning of the deactivation; while the higher conversion (≥85%) of Pt Mo BM can last for ca. 12 h (Figure 9B). The induction period before 6 h of both of the Pt Mo catalysts could be caused by the gradual carburization of MoO<sub>3</sub> to form Mo<sub>2</sub>C, which is also an effective promoter in the aromatization of several hydrocarbons [11,14,15]. Accordingly, the higher yield (ca. 70 wt.%) to BTX for 6 h is observed on the Pt Mo BM catalyst. After the comparison, Pt Mo BM shows both a higher activity and longer stability than the Pt Mo IMP catalyst.

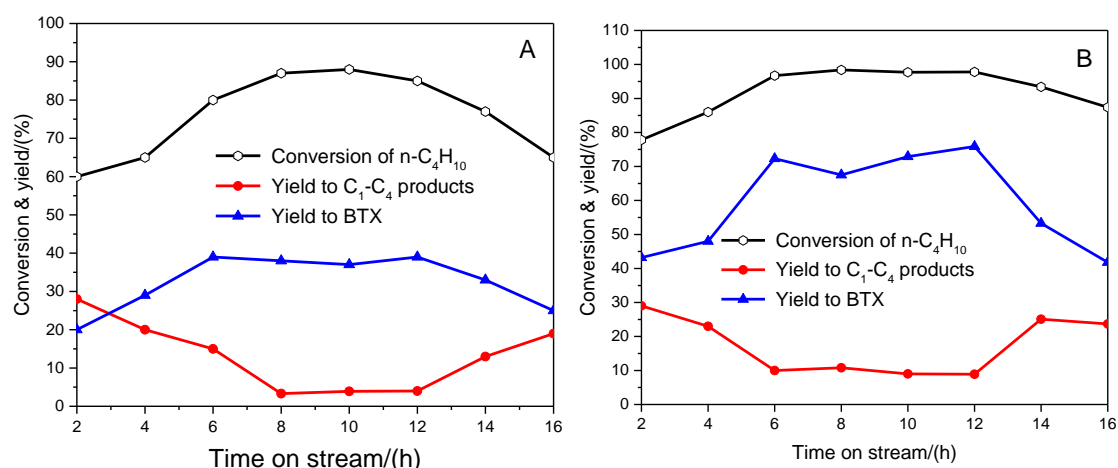


**Figure 9.** Stability (n-butane conversion, yields to benzene, toluene, and xylenes [BTX] and gas products) of Pt Mo IMP (A) and Pt Mo BM (B) catalyst with time-on-stream (TOS).

## 3. Materials and Methods

### 3.1. Catalyst Preparation

Two reference catalysts (PtSn/MoK/ZSM-5 and PtSn/GaK/ZSM-5) were prepared by the step impregnation (IMP) method, according to the literature [29,32,58]. The ZSM-5 zeolite support with a SiO<sub>2</sub>/Al<sub>2</sub>O<sub>3</sub> molar ratio of 50 in acid form (HZSM-5) was supplied by Nankai University Catalyst Plant, Co. The support powder was subsequently washed with deionized water and calcinated at 500 °C for 4 h. A certain weight of support (3 g) was impregnated with the nominal compositions of 0.5 wt.% for Pt, 1.0 wt.% for Sn, 1.5 wt.% Mo/Ga, and 1.0 wt.% for K, by using chloroplatinic acid (H<sub>2</sub>PtCl<sub>6</sub>·6H<sub>2</sub>O), stannous chloride dehydrates (SnCl<sub>2</sub>·2H<sub>2</sub>O), ammonium molybdate ([NH<sub>4</sub>]<sub>5</sub>Mo<sub>7</sub>O<sub>24</sub>·4H<sub>2</sub>O)/gallium nitrate (Ga[NO<sub>3</sub>]<sub>3</sub>), and potassium chloride (KCl) as precursors, which were supplied by Sinopharm Chemical Reagent Co., Ltd (Shanghai, China). The catalysts slurry was dried at 110 °C and calcinated at 500 °C in a Muffle furnace for 4 h, which were abbreviated as the Pt Mo IMP and Pt Ga IMP catalysts.

In a typical synthesis of ball-milled materials, a certain weight of support (1.5 g) was impregnated with the nominal compositions of 1.0 wt.% for Pt, 2.0 wt.% for Sn, and 2.0 wt.% for K. Then, 3.0 wt.% Mo/Ga was introduced to another 1.5 g support. After being dried at 110 °C and calcinated at 500 °C, the PtSnK/ZSM-5 and Mo(Ga)/ZSM-5 powders, with a mass ratio of the two components of 1:1, were put into a jar with a few stainless steel balls inside, and were then milled fully for 30 min. [17], which were abbreviated as the Pt Mo BM and Pt Ga BM catalysts.

### 3.2. Catalyst Characterization

N<sub>2</sub>-adsorption studies were carried out on Micromeritics TriStar 3020 adsorptive and desorptive apparatus after the samples were pretreated in a vacuum at 350 °C for 15 h. The specific surface area was obtained using the Brunauer–Emmett–Teller (BET) method. The micropore surface area, volume, and average pore diameter were determined from the t-plot method [26,32]. The chemical composition was determined using a PANalytical Axios Petro X-ray fluorescence (XRF) instrument (Malvern Panalytical Ltd., Royston, United Kingdom). The X-ray diffraction (XRD) patterns of the prepared catalysts were obtained on a Rigaku Ultima-IV X-ray powder diffractometer (Rigaku Corporation, Tokyo, Japan). An angular range of  $2\theta$  from 5–45° was recorded. The temperature-programmed reduction (TPR) experiment was measured with a Micromeritics AutoChem 2920 apparatus (Micromeritics Instrument Corp., Norcross, GA, USA) and 10% H<sub>2</sub>/Ar was used at a flow rate of 50 mL/min. The temperature-programmed desorption of ammonia (NH<sub>3</sub>-TPD) experiment was measured with the same apparatus. Prior to the measurement, the ca. 0.2 g samples were pretreated in He (99.999%, 50 mL/min) at 500 °C for 1 h. After cooling to 120 °C, the gas flow was switched to 10% NH<sub>3</sub> in He for 50 min. The temperature-programmed desorption of the hydrogen (H<sub>2</sub>-TPD) experiment was performed on the apparatus that was described for TPR. The samples were reduced in the flowing 5% H<sub>2</sub>/Ar at 500 °C for 40 min and cooled down to 50 °C for 1 h. The X-ray photoelectron spectrum (XPS) was obtained with an X probe spectrometer (ESCALAB 250 XI). The binding energies of the Pt 4d, Mo 3d, Ga 2p, and Sn 3d peaks were referenced to the C 1s peak at 284.8 eV. The CO Fourier Transform infrared ray spectroscopy (CO-FTIR) was performed on a Bruker Vertex 70 infrared spectrometer (Bruker Corporation, Ettlingen, Germany), with a resolution of 4 cm<sup>-1</sup>, and with 128 scans for each spectrum. [59]. The thermogravimetric analysis (TG) of the used catalysts was performed on a TG 209 F1 thermogravimetric analyzer (NETZSCH).

### 3.3. Catalyst Evaluation

The catalytic aromatization reaction was performed in the micro-catalytic reactor. Before evaluation, the sample was pressed, crushed, and sieved to 40–60 mesh particles. Then, 1 mL of the catalyst particles were located in a fixed bed stainless reactor with 320 mm length and 12 mm diameter, and pretreated at 500 °C in a H<sub>2</sub> (99.99%) flow of 20 mL/min for 2 h. Then, it was adjusted to the desired temperature range of 400–500 °C. When the temperature was stable, the feed with an n-butane/methanol ratio of 60/40 was introduced when the pressure was 0.2 MPa, and the weight hourly space velocity of CH<sub>2</sub> (WHSV [CH<sub>2</sub>]) was 0.6 h<sup>-1</sup>. The n-butane/methanol ratio denotes the carbon molar ratio of n-butane to methanol [9,10]. The main products were on line analyzed using a Shanghai Wuhaio GC 9560 gas chromatograph (KB-PONA capillary column, 50 m × 0.25 mm × 0.50 μm, FID detector). The tubing between the reactor and the GC was heated to 150 °C so as to prevent the condensation of heavy products. The conversion of n-butane and the corresponding product distribution are calculated using the method described in the literature [9,10]. The reaction equipment is shown in Figure S1. The n-C<sub>4</sub>H<sub>10</sub> conversion (*X*) and selectivity (*S*) of the products, by weight, were calculated using the following equations:

$$X(\text{n-C}_4\text{H}_{10})\% = (\text{n-C}_4\text{H}_{10} \text{ mass in feed} - \text{n-C}_4\text{H}_{10} \text{ mass in product}) / (\text{n-C}_4\text{H}_{10} \text{ mass in feed}) \times 100\%$$

$$S(\text{product})\% = (\text{product mass}) / (\text{CH}_2 \text{ mass in feed} - (\text{n-C}_4\text{H}_{10} + \text{CH}_3\text{OH}) \text{ mass in product}) \times 100\%$$

The yield ( $Y$ ) was simply obtained by multiplying the conversion by the selectivity. The target aromatic product  $i$  ( $i$  = benzene, toluene, xylenes + ethylbenzene, and  $C_9^+$  aromatics) selectivity ( $S[\text{Aro. } i]$ ) in the liquid product (Aro. mass) in Tables was calculated as follows:

$$S(\text{Aro. } i)\% = (\text{Aro. } i \text{ mass})/(\text{Aro. mass}) \times 100\%$$

#### 4. Conclusions

It should be a good approach to combine the endothermic aromatization of alkane with the exothermic aromatization of methanol. The ball-milling (BM) method benefits the stabilization and dispersion of the metallic particles for the preparation of the PtSnK–Mo/ZSM-5 catalyst. Based on the TPR,  $H_2$ -TPD, XPS, and CO-FTIR results, the Pt–SnO<sub>x</sub> and MoO<sub>x</sub> species were formed separately on the BM sample. During the co-aromatization with an n-butane/methanol ratio of 60/40, the yield of the aromatics is 59 wt.% at a n-butane conversion of 86% under the best operating conditions of 475 °C, 0.2 MPa, and 0.6 h<sup>−1</sup>, over the Pt Mo BM catalyst with less coke formation (80 mg/g.cat.), and the higher conversion ( $\geq 85\%$ ) can last for ca. 12 h of TOS. More weak acid sites of the Pt Mo sample also contribute to the aromatics formation with less light alkanes formation. However, the effect of the impregnation (IMP) method is not satisfying with both lower activity (65%) and yield (38 wt.%) of aromatics with stability of only 6 h. For the Pt Ga catalysts, the coke formation is obvious; while the slow loss of activity suggests that the BM method can restrain the coke deposition on the Pt–SnO<sub>x</sub> species due to a certain distance between the Pt–SnO<sub>x</sub> and GaO<sub>x</sub> species on the surface of ZSM-5.

**Supplementary Materials:** The following are available online at <http://www.mdpi.com/2073-4344/8/8/307/s1>, Figure S1: Schematic diagram of the co-aromatization apparatus and online analysis with two gas chromatographs used in this work, Figure S2: XRD patterns of Pt Mo, Pt Ga and ZSM-5 samples, Figure S3: N<sub>2</sub> adsorption-desorption isotherms (A) and pore size distribution (B) for Pt Mo BM, Pt Mo IMP, Pt Ga BM and Pt Ga IMP samples, Figure S4: NH<sub>3</sub>-TPD profiles of Pt Mo BM, Pt Mo IMP, Pt Ga BM, Pt Ga IMP and ZSM-5, Figure S5: XPS spectra of Sn 3d<sub>5/2</sub> and Sn 3d<sub>3/2</sub> regions for Pt Mo/Ga samples. All samples are reduced at 500 °C, Figure S6: Effect of reaction temperature on n-butane conversion, selectivity to aliphatics (A) and selectivity to aromatics (B) over Pt Ga IMP. C<sub>5</sub>H<sub>10</sub> in aliphatics was used to simplify molar calculations for C<sub>5</sub> aliphatics, Figure S7: Effect of reaction temperature on n-butane conversion, selectivity to aliphatics (A) and selectivity to aromatics (B) over Pt Ga BM. C<sub>5</sub>H<sub>10</sub> in aliphatics and C<sub>10</sub>H<sub>14</sub> in aromatics were used to simplify molar calculations for C<sub>5</sub> aliphatics and C<sub>10+</sub> aromatics, Figure S8: TG profiles of used Pt Mo BM, Pt Mo IMP, Pt Ga BM and Pt Ga IMP samples under air, Figure S9: Effect of Mo content on evolution of the in situ CO-FTIR spectra of Pt Mo BM catalysts under N<sub>2</sub> during 40 min. All samples are in situ reduced at 500 °C, Table S1: Textural properties of Pt Mo BM, Pt Mo IMP, Pt Ga BM, Pt Ga IMP and ZSM-5, Table S2: ZSM-5 catalyst performance in the aromatization of cofeeding n-butane with methanol, Table S3: Effect of Mo content on the catalytical performance of Pt Mo catalysts in the aromatization of cofeeding n-butane with methanol, Table S4: Effect of cofeeding composition on the catalytical performance of Pt Mo (1.5 wt.%) BM catalyst in the aromatization of cofeeding n-butane with methanol.

**Author Contributions:** Data curation, L.Z.; funding acquisition, Y.L.; investigation, J.Z.; methodology, X.H.; supervision, W.F.; writing (original draft), K.Y.; writing (review and editing), W.L.

**Acknowledgments:** This work was financially supported by the National Natural Science Foundation of China (No. 21703179 and No. 21473143) and the Fundamental Research Funds for the Central Universities of China (No. 20720170103).

**Conflicts of Interest:** The authors declare no conflict of interest.

#### References

1. Mi, D. Analysis of domestic and foreign aromatics production and market supply and demand pricing (Chinese version). *Chem. Ind.* **2017**, *35*, 59–64.
2. Dai, W.; Yang, L.; Wang, C.; Wang, X.; Wu, G.; Guan, N.; Obenaus, U.; Hunger, M.; Li, L. Effect of n-Butanol Cofeeding on the Methanol to Aromatics Conversion over Ga-Modified Nano H-ZSM-5 and Its Mechanistic Interpretation. *ACS Catal.* **2018**, *8*, 1352–1362. [CrossRef]
3. Jia, Y.; Wang, J.; Zhang, K.; Feng, W.; Liu, S.; Ding, C.; Liu, P. Nanocrystallite self-assembled hierarchical ZSM-5 zeolite microsphere for methanol to aromatics. *Microporous Mesoporous Mater.* **2017**, *247*, 103–115. [CrossRef]

4. Conte, M.; Lopez-Sanchez, J.A.; He, Q.; Morgan, D.J.; Ryabenkova, Y.; Bartley, J.K.; Carley, A.F.; Taylor, S.H.; Kiely, C.J.; Khalid, K.; et al. Modified zeolite ZSM-5 for the methanol to aromatics reaction. *Catal. Sci. Technol.* **2012**, *2*, 105–112. [[CrossRef](#)]
5. Lai, P.C.; Chen, C.H.; Hsu, H.Y.; Lee, C.H.; Lin, Y.C. Methanol aromatization over Ga-doped desilicated HZSM-5. *RSC Adv.* **2016**, *6*, 67361–67371. [[CrossRef](#)]
6. Xin, Y.; Qi, P.; Duan, X.; Lin, H.; Yuan, Y. Enhanced Performance of Zn–Sn/HZSM-5 Catalyst for the Conversion of Methanol to Aromatics. *Catal. Lett.* **2013**, *143*, 798–806. [[CrossRef](#)]
7. Zhang, J.; Qian, W.; Kong, C.; Wei, F. Increasing para-Xylene Selectivity in Making Aromatics from Methanol with a Surface-Modified Zn/P/ZSM-5 Catalyst. *ACS Catal.* **2015**, *5*, 2982–2988. [[CrossRef](#)]
8. Mier, D.; Aguayo, A.T.; Gayubo, A.G.; Olazar, M.; Bilbao, J. Synergies in the production of olefins by combined cracking of n-butane and methanol on a HZSM-5 zeolite catalyst. *Chem. Eng. J.* **2010**, *160*, 760–769. [[CrossRef](#)]
9. Song, C.; Liu, S.; Li, X.; Xie, S.; Liu, Z.; Xu, L. Influence of reaction conditions on the aromatization of cofeeding n-butane with methanol over the Zn loaded ZSM-5/ZSM-11 zeolite catalyst. *Fuel Process. Technol.* **2014**, *126*, 60–65. [[CrossRef](#)]
10. Song, C.; Liu, K.; Zhang, D.; Liu, S.; Li, X.; Xie, S.; Xu, L. Effect of cofeeding n-butane with methanol on aromatization performance and coke formation over a Zn loaded ZSM-5/ZSM-11 zeolite. *Appl. Catal. A* **2014**, *470*, 15–23. [[CrossRef](#)]
11. Fila, V.; Bernauer, M.; Bernauer, B.; Sobalik, Z. Effect of addition of a second metal in Mo/ZSM-5 catalyst for methane aromatization reaction under elevated pressures. *Catal. Today* **2015**, *256*, 269–275. [[CrossRef](#)]
12. Tshabalala, T.E.; Scurrall, M.S. Aromatization of n-hexane over Ga, Mo and Zn modified H-ZSM-5 zeolite catalysts. *Catal. Commun.* **2015**, *72*, 49–52. [[CrossRef](#)]
13. Barthos, R.; Solymosi, F. Aromatization of n-heptane on Mo<sub>2</sub>C-containing catalysts. *J. Catal.* **2005**, *235*, 60–68. [[CrossRef](#)]
14. Solymosi, F.; Széchenyi, A. Aromatization of n-butane and 1-butene over supported Mo<sub>2</sub>C catalyst. *J. Catal.* **2004**, *223*, 221–231. [[CrossRef](#)]
15. Barthos, R.; Bánsági, T.; Zakar, T.S.; Solymosi, F. Aromatization of methanol and methylation of benzene over Mo<sub>2</sub>C/ZSM-5 catalysts. *J. Catal.* **2007**, *247*, 368–378. [[CrossRef](#)]
16. James, S.L.; Adams, C.J.; Bolm, C.; Braga, D.; Collier, P.; Friščić, T.; Grepioni, F.; Harris, K.D.M.; Hyett, G.; Jones, W. Mechanochemistry: Opportunities for new and cleaner synthesis. *Chem. Soc. Rev.* **2011**, *41*, 413–447. [[CrossRef](#)] [[PubMed](#)]
17. Cheng, K.; Gu, B.; Liu, X.; Kang, J.; Zhang, Q.; Wang, Y. Direct and Highly Selective Conversion of Synthesis Gas into Lower Olefins: Design of a Bifunctional Catalyst Combining Methanol Synthesis and Carbon–Carbon Coupling. *Angew. Chem. Int. Ed.* **2016**, *128*, 4803–4806. [[CrossRef](#)]
18. Lin, Q.; Guo, Z.; Pan, L.; Xiang, X. Zn-Cr double metal cyanide catalysts synthesized by ball milling for the copolymerization of CO<sub>2</sub>/propylene oxide, phthalic anhydride/propylene oxide, and CO<sub>2</sub>/propylene oxide/phthalic anhydride. *Catal. Commun.* **2015**, *64*, 114–118.
19. Pineda, A.; Balu, A.M.; Campelo, J.M.; Romero, A.A.; Carmona, D.; Balas, F.; Santamaria, J.; Luque, R. A dry milling approach for the synthesis of highly active nanoparticles supported on porous materials. *ChemSusChem* **2011**, *4*, 1561–1565. [[CrossRef](#)] [[PubMed](#)]
20. Caeiro, G.; Carvalho, R.H.; Wang, X.; Lemos, M.A.N.D.A.; Lemos, F.; Guisnet, M.; Ribeiro, F.R. Activation of C<sub>2</sub>–C<sub>4</sub> alkanes over acid and bifunctional zeolite catalysts. *J. Mol. Catal. A* **2006**, *255*, 131–158. [[CrossRef](#)]
21. Sattler, J.J.; Ruizmartinez, J.; Santillanjimenez, E.; Weckhuysen, B.M. Catalytic dehydrogenation of light alkanes on metals and metal oxides. *Chem. Rev.* **2014**, *114*, 10613–10653. [[CrossRef](#)] [[PubMed](#)]
22. Zhu, X.; Liu, S.; Song, Y.; Xu, L. Butene Catalytic Cracking to Propene and Ethene over Potassium Modified ZSM-5 Catalysts. *Catal. Lett.* **2005**, *103*, 201–210. [[CrossRef](#)]
23. Epelde, E.; Santos, J.I.; Florian, P.; Aguayo, A.T.; Gayubo, A.G.; Bilbao, J.; Castaño, P. Controlling coke deactivation and cracking selectivity of MFI zeolite by H<sub>3</sub>PO<sub>4</sub> or KOH modification. *Appl. Catal. A* **2015**, *505*, 105–115. [[CrossRef](#)]
24. Song, Y.; Zhu, X.; Xie, S.; Wang, Q.; Xu, L. The Effect of Acidity on Olefin Aromatization over Potassium Modified ZSM-5 Catalysts. *Catal. Lett.* **2004**, *97*, 31–36. [[CrossRef](#)]
25. Zhang, C.; Li, S.; Wu, G.; Gong, J. Synthesis of stable Ni–CeO<sub>2</sub> catalysts via ball-milling for ethanol steam reforming. *Catal. Today* **2014**, *233*, 53–60. [[CrossRef](#)]

26. Wan, Z.; Wu, W.; Li, G.; Wang, C.; Yang, H.; Zhang, D. Effect of SiO<sub>2</sub>/Al<sub>2</sub>O<sub>3</sub> ratio on the performance of nanocrystal ZSM-5 zeolite catalysts in methanol to gasoline conversion. *Appl. Catal. A* **2016**, *523*, 312–320. [[CrossRef](#)]
27. Zhang, Y.; Zhou, Y.; Shi, J.; Zhou, S.; Sheng, X.; Zhang, Z.; Xiang, S. Comparative study of bimetallic Pt-Sn catalysts supported on different supports for propane dehydrogenation. *J. Mol. Catal. A* **2014**, *381*, 138–147. [[CrossRef](#)]
28. Morán, C.; González, E.; Sánchez, J.; Solano, R.; Carruyo, G.; Moronta, A. Dehydrogenation of ethylbenzene to styrene using Pt, Mo, and Pt-Mo catalysts supported on clay nanocomposites. *J. Colloid Interface Sci.* **2007**, *315*, 164–169. [[CrossRef](#)] [[PubMed](#)]
29. Tshabalala, T.E.; Coville, N.J.; Scurrall, M.S. Dehydroaromatization of methane over doped Pt/Mo/H-ZSM-5 zeolite catalysts: The promotional effect of tin. *Appl. Catal. A* **2014**, *485*, 238–244. [[CrossRef](#)]
30. Meriaudeau, P.; Albano, K.; Naccache, C. Promotion of platinum-based catalysts for methanol synthesis from syngas. *J. Chem. Soc. Faraday Trans. L* **1987**, *83*, 2113–2118. [[CrossRef](#)]
31. Silva, M.A.P.D.; Mellovieira, R.A.; Schmal, M. Interaction between Pt and MoO<sub>3</sub> dispersed over alumina. *Appl. Catal. A* **2000**, *190*, 177–190. [[CrossRef](#)]
32. Zhang, Y.; Zhou, Y.; Yang, K.; Li, Y.; Wang, Y.; Xu, Y.; Wu, P. Effect of hydrothermal treatment on catalytic properties of PtSnNa/ZSM-5 catalyst for propane dehydrogenation. *Microporous Mesoporous Mater.* **2006**, *96*, 245–254. [[CrossRef](#)]
33. Kolobova, E.; Pestryakov, A.; Mamontov, G.; Kotolevich, Y.; Bogdanchikova, N.; Farias, M.; Vosmerikov, A.; Vosmerikova, L.; Corberan, V.C. Low-temperature CO oxidation on Ag/ZSM-5 catalysts: Influence of Si/Al ratio and redox pretreatments on formation of silver active sites. *Fuel* **2017**, *188*, 121–131. [[CrossRef](#)]
34. Muddada, N.B.; Olsbye, U.; Fuglerud, T.; Vidotto, S.; Marsella, A.; Bordiga, S.; Gianolio, D.; Leofanti, G.; Lamberti, C. The role of chlorine and additives on the density and strength of Lewis and Brønsted acidic sites of  $\gamma$ -Al<sub>2</sub>O<sub>3</sub> support used in oxychlorination catalysis: A FTIR study. *J. Catal.* **2011**, *284*, 236–246. [[CrossRef](#)]
35. Ro, I.B.; Aragao, Z.J.; Brentzel, Y.; Liu, K.R.; Rivera-Dones, M.R.; Ball, D.; Zanchet, G.W.; Huber, J.A. Dumesic, Intrinsic Activity of Interfacial Sites for Pt-Fe and Pt-Mo Catalysts in the Hydrogenation of Carbonyl Groups. *Appl. Catal. B* **2018**, *231*, 182–190. [[CrossRef](#)]
36. Matsuda, T.; Ohno, T.; Hiramatsu, Y.; Li, Z.; Sakagami, H.; Takahashi, N. Effects of the amount of MoO<sub>3</sub> on the catalytic properties of H<sub>2</sub>-reduced Pt/MoO<sub>3</sub>-SiO<sub>2</sub> for heptane isomerization. *Appl. Catal. A* **2009**, *362*, 40–46. [[CrossRef](#)]
37. Pidko, E.A.; Hensen, E.J.M.; Santen, R.A.V. Dehydrogenation of Light Alkanes over Isolated Gallyl Ions in Ga/ZSM-5 Zeolites. *J. Phys. Chem. C* **2007**, *111*, 13068–13075. [[CrossRef](#)]
38. Yoshida, H.; Narisawa, S.; Fujita, S.; Ruixia, L.; Arai, M. In situ FTIR study on the formation and adsorption of CO on alumina-supported noble metal catalysts from H<sub>2</sub> and CO<sub>2</sub> in the presence of water vapor at high pressures. *Phys. Chem. Chem. Phys.* **2012**, *14*, 4724–4733. [[CrossRef](#)] [[PubMed](#)]
39. Brandt, R.K.; Sorbello, R.S.; Greenler, R.G. Site-specific, coupled-harmonic-oscillator model of carbon monoxide adsorbed on extended, single-crystal surfaces and on small crystals of platinum. *Surf. Sci.* **1992**, *271*, 605–615. [[CrossRef](#)]
40. Ding, K.; Gulec, A.; Johnson, A.M.; Schweitzer, N.M.; Stucky, G.D.; Marks, L.D.; Stair, P.C. Identification of active sites in CO oxidation and water-gas shift over supported Pt catalysts. *Science* **2015**, *350*, 189–192. [[CrossRef](#)] [[PubMed](#)]
41. Pattamakomsan, K.; Ehret, E.; Morfin, F.; Gélin, P.; Jugnet, Y.; Prakash, S.; Bertolini, J.C.; Panpranot, J.; Aires, F.J.C.S. Selective hydrogenation of 1,3-butadiene over Pd and Pd-Sn catalysts supported on different phases of alumina. *Catal. Today* **2011**, *164*, 28–33. [[CrossRef](#)]
42. Busca, G. Spectroscopic characterization of the acid properties of metal oxide catalysts. *Catal. Today* **1998**, *41*, 191–206. [[CrossRef](#)]
43. Daturi, M.; Appel, L.G. Infrared Spectroscopic Studies of Surface Properties of Mo/SnO<sub>2</sub> Catalyst. *J. Catal.* **2002**, *209*, 427–432. [[CrossRef](#)]
44. Seo, H.; Lee, J.K.; Hong, U.G.; Park, G.; Yoo, Y.; Lee, J.; Chang, H.; Song, I.K. Direct dehydrogenation of n-butane over Pt/Sn/M/ $\gamma$ -Al<sub>2</sub>O<sub>3</sub> catalysts: Effect of third metal (M) addition. *Catal. Commun.* **2014**, *47*, 22–27. [[CrossRef](#)]

45. Jaroszevska, K.; Masalska, A.; Marek, D.; Grzechowiak, J.R.; Zemska, A. Effect of support composition on the activity of Pt and PtMo catalysts in the conversion of n-hexadecane. *Catal. Today* **2014**, *223*, 76–86. [[CrossRef](#)]
46. Serrano-Ruiz, J.C.; Huber, G.W.; Sánchez-Castillo, M.A.; Dumesic, J.A.; Rodríguez-Reinoso, F.; Sepúlveda-Escribano, A. Effect of Sn addition to Pt/CeO<sub>2</sub>-Al<sub>2</sub>O<sub>3</sub> and Pt/Al<sub>2</sub>O<sub>3</sub> catalysts: An XPS, <sup>119</sup>Sn Mössbauer and microcalorimetry study. *J. Catal.* **2006**, *241*, 378–388. [[CrossRef](#)]
47. Li, Z.; Gao, L.; Zheng, S. Investigation of the dispersion of MoO<sub>3</sub> onto the support of mesoporous silica MCM-41. *Appl. Catal. A* **2002**, *236*, 163–171. [[CrossRef](#)]
48. Choi, J.G.; Thompson, L.T. XPS study of as-prepared and reduced molybdenum oxides. *Appl. Surf. Sci.* **1996**, *93*, 143–149. [[CrossRef](#)]
49. Moulder, J.F.; Chastain, J.; King, R.C., Jr. Handbook of X-ray photoelectron spectroscopy: A reference book of standard spectra for identification and interpretation of XPS data. *Chem. Phys. Lett.* **1992**, *220*, 7–10.
50. Nowak, J. Quartararo, Effect of H<sub>2</sub>-O<sub>2</sub> pre-treatments on the state of gallium in Ga/H-ZSM-5 propane aromatisation catalysts. *Appl. Catal. A* **2003**, *251*, 107–120. [[CrossRef](#)]
51. Wen, Z.; Yang, D.; He, X.; Li, Y.; Zhu, X. Methylation of benzene with methanol over HZSM-11 and HZSM-5: A density functional theory study. *J. Mol. Catal. A* **2016**, *424*, 351–357. [[CrossRef](#)]
52. Gabrienko, A.A.; Arzumanov, S.S.; Freude, D.; Stepanov, A.G. Propane Aromatization on Zn-Modified Zeolite BEA Studied by Solid-State NMR In Situ. *J. Phys. Chem. C* **2010**, *114*, 12681–12688. [[CrossRef](#)]
53. Karp, E.M.; Silbaugh, T.L.; Campbell, C.T. Energetics of Adsorbed CH<sub>3</sub> and CH on Pt(111) by Calorimetry: Dissociative Adsorption of CH<sub>3</sub>I. *J. Phys. Chem. C* **2013**, *117*, 6325–6336. [[CrossRef](#)]
54. Akhtar, M.N.; Al-Yassir, N.; Al-Khattaf, S.; Čejka, J. Aromatization of alkanes over Pt promoted conventional and mesoporous gallosilicates of MEL zeolite. *Catal. Today* **2012**, *179*, 61–72. [[CrossRef](#)]
55. Martínez-Espin, J.S.; de Wispelaere, K.; Erichsen, M.W.; Svelle, S.; Janssens, T.V.W.; van Speybroeck, V.; Beato, P.; Olsbye, U. Benzene co-reaction with methanol and dimethyl ether over zeolite and zeotype catalysts: Evidence of parallel reaction paths to toluene and diphenylmethane. *J. Catal.* **2017**, *349*, 136–148. [[CrossRef](#)]
56. Wei, Z.; Chen, L.; Cao, Q.; Wen, Z.; Zhou, Z.; Xu, Y.; Zhu, X. Steamed Zn/ZSM-5 catalysts for improved methanol aromatization with high stability. *Fuel Process. Technol.* **2017**, *162*, 66–77. [[CrossRef](#)]
57. Song, C.; Li, X.; Zhu, X.; Liu, S.; Chen, F.; Liu, F.; Xu, L. Influence of the state of Zn species over Zn-ZSM-5/ZSM-11 on the coupling effects of cofeeding n-butane with methanol. *Appl. Catal. A* **2016**, *519*, 48–55. [[CrossRef](#)]
58. Baldovino-Medrano, V.G.; Giraldo, S.A.; Centeno, A. The functionalities of Pt-Mo catalysts in hydrotreatment reactions. *Fuel* **2010**, *89*, 1012–1018. [[CrossRef](#)]
59. Yang, K.; Liu, C. Hydrogenation of isoprene over gold supported on CeO<sub>2</sub>, ZrO<sub>2</sub>, SiO<sub>2</sub> and N-SiO<sub>2</sub>. *J. Ind. Eng. Chem.* **2015**, *28*, 161–170. [[CrossRef](#)]

